International Journal of Computer Information Systems and Industrial Management Applications
ISSN 2150-7988 Volume 18(2s) 2026 pp. 42-58
https://doi.org/10.70917/ijcisim-2026-2064
Article

BRAIN TUMOR SEGMENTATION USING DUAL FUSION ENHANCED DEFORMABLE CONVOLUTIONAL NETWORK AND ARTIFICIAL LEMSTAR OPTIMIZATION

B. Naga Rajesh[1], Gopalakrishna K[2]

[1]Department of Electronics Engineering, JAIN (Deemed-to-be University), Bengaluru, India. Email: nagarajesh87@gmail.com
[2]Department of Electronics and Communication Engineering, JAIN (Deemed-to-be University), Bengaluru, India. Email: k.gopalakrishna@jainuniversity.ac.in
Corresponding Author: B. Naga Rajesh[1]* (Email: nagarajesh87@gmail.com)

Abstract: Brain tumors are highly aggressive and pose a serious threat to life expectancy across varied demographic groups. Detecting them early allows for timely treatment, which greatly improves survival chances. However, segmentation is complicated by similar imaging intensities, irregular tumor shapes, and unclear boundaries. Hence, this paper presents a new method using the Dual Fusion with Enhanced Deformable Convolution Network (DFEDC) and Artificial LemStar Optimization Algorithm (ALStarOA) for segmenting brain tumors using Magnetic Resonance Images (MRI). Firstly, the MRI image is given to image denoising using Spatial Domain Filtering (SDF). Then, DFEDC is utilized to perform brain tumor region segmentation, and the loss function of DFEDC is modified by using the Exponential Baikal Loss. DFEDC is trained by exploiting ALStarOA, which is developed by combining StarFish Optimization Algorithm (SFOA) and Artificial Lemming Algorithm (ALA). Experimental analysis shows that the proposed methodology outperforms with a higher segmentation accuracy of 97.467%, dice coefficient of 97.777%, and Intersection Over Union (IOU) of 98.279%. .
Keywords: Segmentation, Deep Learning, MRI, Deformable model, Artificial LemStar Optimization.

1. Introduction

Brain tumors represent an uncontrolled pathological proliferation of cells within the brain [1]. Brain tumors rank among the most prevalent causes of mortality worldwide. Brain tumors are broadly categorized into cancerous or malignant and noncancerous or benign types. Malignant tumors present a heightened clinical concern due to their invasive nature and tendency to infiltrate adjacent brain structures, often leading to a poorer prognosis. Timely diagnosis and therapeutic intervention are essential as brain tumors often arise from neighboring tissues and exhibit progressive expansion. Early treatment markedly enhances

clinical outcomes and patient survival rates [2], [3]. To enhance diagnostic precision for brain tumor kinds, it is crucial to construct an advanced technique that synthesizes dynamic and structural characteristics across a continuum of pathological severity [4]. Medical image segmentation is a critical component of clinical diagnostics, yet, it remains challenging task due to low image contrast, various noise

artifacts, and the presence of ambiguous or indistinct boundaries [5], [6].

Tumors such as meningiomas are generally well-defined and difficult to segmentation. In contrast, gliomas and glioblastomas present significant challenges due to their diffuse nature, low contrast, and infiltrative growth patterns, often accompanied by surrounding edema and irregular,

tentacle-like extensions that obscure clear boundaries [7], [8]. Although significant progress has been made, accurate segmentation of brain tumors continues to be a complex problem. Contributing factors for inaccurate segmentation include uncertainty in tumor localization and shape, low-contrast imaging conditions, annotation bias, and disproportionate data distribution [9]. The detection and segmentation of brain tumors offer critical insights into anatomical structures and pathological regions essential for therapeutic planning and longitudinal patient monitoring [10], [11]. Deformable models are commonly used in medical image processing because of their ability to adapt to irregular shapes to accurately trace tumor boundaries [12], [13].

Classical Machine Learning (ML) algorithms have long been integral to CAD systems, particularly for classification tasks. Owing to the remarkable performance of advanced Deep Learning (DL) techniques, numerous DL-based approaches are adopted for brain tumor segmentation. These methods enable automatic feature extraction and consistently deliver high accuracy and robust segmentation outcomes [9]. DL techniques, particularly Convolutional Neural Networks (CNNs), have become an effective approach in brain tumor segmentation in recent years. These models benefit from large-scale datasets and typically require minimal preprocessing as compared to traditional ML methods. Although considerable advancements have been made in CNN architectures and hybrid modeling approaches, achieving concurrent segmentation and classification of multiple cancerous lesions in MRI continues to pose a substantial challenge. Moreover, classification performance is constrained by limited tumor class diversity, typically restricted to four or fewer categories, leading to increased susceptibility to overfitting and reduced generalizability across broader clinical scenarios [14]. Enhanced DL models, multi-modal imaging integration, and transfer learning have significantly boosted diagnostic accuracy.

Nevertheless, persistent challenges, including the scarcity of annotated datasets, limited interpretability of Artificial Intelligence (AI) driven models, and the demand for real-time clinical integration, continue to hinder widespread implementation.

The novel approach of this paper is Dual Fusion with Enhanced Deformable Convolution Network with Artificial LemStar Optimization Algorithm for brain tumor segmentation. Initially, the MRI scans retrieved from the database are subjected to image denoising using SDF. Subsequently, segmenting tumor region is carried out by DFEDC framework, wherein the loss function is customized through the proposed Exponential Baikal Loss. This new loss function is formulated by incorporating Baikal Loss with Exponential Loss. Furthermore, the DFEDC model is learned using ALStarOA, which combines the strengths of SFOA and ALA to enhance model robustness and training efficiency.

2. Related Work

Zarenia, E., *et al.* [2] developed a Hierarchical Multiscale Deformable Attention Module (MS-DAM) for automated multi-class MRI brain tumor classification and segmentation. This technique has high stability, robustness and reduced data loss. However, the model did not adequately address key aspects such as computational efficiency, multimodal imaging integration, and the development of hybrid DL frameworks that combine MRI data with medical biomarkers to enable more holistic tumor diagnostics. An Efficient Net- Enhanced UNet was proposed by Tiwary P K *et al.* [13] for MRI brain tumor segmentation. This technique required less training time, enhanced segmentation precision, and reduced overfitting issues. However, this approach was not suitable for real-time applications. Almufareh, M.F *et al.* [15] established a method based on You Only Look Once versions (YOLOv5 and YOLOv7) for automated brain tumor segmentation and classification in MRI. This model had better performance, reduced overfitting issues, and had potential to handle diverse sources. The key limitation of this work was its reliance on a single dataset, and the substantial computational incomes needed to assess larger databases. A technique using UNet was developed by Obayya M *et al.* [16]. UNet was more effective in attaining high efficiency with reduced computational complexity, increased flexibility, and minimized information loss. Meanwhile, this technique failed to employ segmentation-specific metrics, which are pivotal for evaluating how accurately tumor margins are identified and for addressing class imbalance issues. Multi-Modal network was designed by Jeslin T and Thanya T [3]. This approach had better interpretability, enhanced efficiency, robustness, and strong discriminatory power. However, the model demonstrated limitations in multimodal integration, failing to incorporate MRI data with complementary imaging methodology, like CT scan or Positron Emission Tomography (PET). Li Z *et al.* [17] devised a Local-Global Modeling + Deformable Adaptive Perception with Reconstruction-Driven Key Information Mining (LGM+DAP+RDKIM). This approach had robust segmentation, enhanced performance, reduced computational complexities. But it is failed to improve the performance using advanced DL techniques. The Barely-Supervised Learning (BSL) framework was proposed by Ma. X *et al.* [18] and this method effectively addressed class imbalance issues but minimized energy consumption, and had a lower error rate. Nonetheless, the technique

lacked attention to enhancing model adaptability for irregular and complex tumor morphologies. Xiong M *et al.* [19] introduced YOLO- Brain Tumor (YOLO-BT). This approach had better generalization, less memory consumption and reduced computational complexities. But this technique did not contribute intelligent diagnostic platforms developments, applicable through diverse disease categories, nor did it facilitate the practical integration and deployment of AI technologies within clinical settings. The following are the key challenges of the existing segmentation models.

The Unet model in [16] enabled efficient multi-scale feature extraction, and effectively distinguished between tumor subregions, potentially enabling real-time diagnostics, but it failed to normalize pixel intensity fluctuations that interfere with algorithmic segmentation. The MultiModNet model developed in [3] ensured precise alignment of anatomical structures and comprehensive capture of tumor characteristics by utilizing the Fast Diffeomorphic Image Registration (FDIR) algorithm and the Deep Gabor Filters (D-GF) for feature extraction. However, it failed to capture fine spatial details and contextual information, to resolve complex segmentation cases.

The LGM+DAP+RDKIM framework in [17] utilized local–global modeling, which explicitly discovered and leveraged the internal correlations within modalities, thereby enhancing the feature representation capability of the encoder, but it did not produce stronger gradient signals at critical regions to help deformable models avoid local minima and adhere closely to tumor boundaries. In [19], the YOLO-BT algorithm effectively reduced the likelihood of missed diagnoses and supported clinical decision-making, however, it failed to enhance feature representation or designing more robust loss functions to improve sensitivity. Real-time challenges such as noise, intensity inhomogeneity, irregular tumor shapes, and weak boundaries hinder for accurate segmentation.

3. Proposed Methodology

This paper presents a novel methodology, called DFEDC_ALStarOA for segmenting the brain tumors. Fig. 1 illustrates the proposed model. Initially, MRI images acquired from the database are subjected to image denoising using SDF [20] to reduce noise and enhance image clarity. Following denoising, tumor region segmentation is accomplished using the DFEDC framework [21], where the loss function is modified utilizing Exponential Baikal Loss constructed by integrating Baikal Loss [22] with Exponential Loss [23]. Additionally, the DFEDC model is trained using a newly proposed optimization algorithm, ALStarOA, which is developed by combining ALA [24] and SFOA [25] to boost training efficiency and model robustness.

Let us assume that the images used for segmenting brain tumors are assimilated from the MRI-based brain tumor image dataset Q, which is given by,

$$Q = \left\{V_1, V_2, ..., V_y, ..., V_z\right\} \tag{1}$$

where, V_y characterizes the y^{th} MRI input image, and image count in dataset is signified as z.

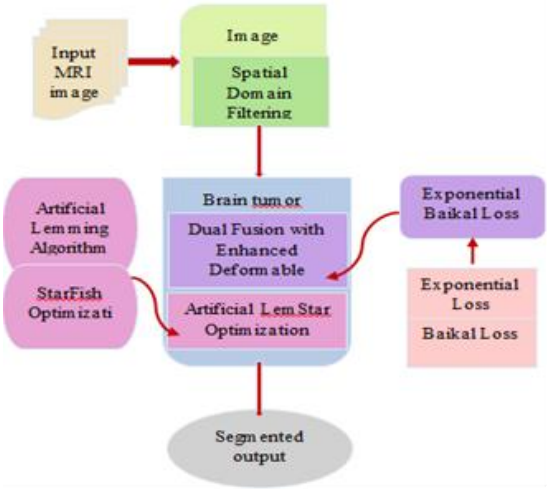

Fig. 1. Proposed DFEDC_ALStarOA model for MRI-based segmenting of brain tumors.

Image denoising using Spatial Domain Filtering

Image denoising is the procedure for eliminating noise from MRI scans to enhance clarity and quality of the image. Here, the image V_y is fed as input for image denoising, which is performed by using SDF [20]. SDF enhances image clarity, reduces high-frequency noise, preserves edges, and improves segmentation accuracy. Here, high-frequency component selection is determined exclusively by the pheromone levels of the traversal routes and heuristic-based decision-making. During the process, pixel r selects its next node using a probabilistic action selection mechanism, which computes the likelihood of transitioning from the current node s to the subsequent node t and is expressed by,

$$a_{st}^{r} = \frac{\left[L_{st}\right]^{\alpha}\left[l_{st}\right]^{\beta}}{\sum_{Fs}^{r}\left[L_{st}\right]^{\alpha}\left[l_{st}\right]^{\beta}} \; if \; t \in F_s^r \tag{2}$$

where, a_{st}^{r} represents probability of pixel r moving from node s to node t, essence of arc from the node s to node t is symbolized by L_{st}, the neighboring node for a specific pixel is indicated as F_s^r, which is assumed to be on the node s, and l_{st} represents heuristics for moving from the node s to node t. The denoised output gained is specified as W.

Dual Fusion with Enhanced Deformable Convolution Network with Artificial LemStar Optimization Algorithm

Deformable models serve as a crucial tool in brain tumor segmentation, as they provide flexible mechanisms for delineating intricate anatomical features that static models or basic thresholding often fail to capture. Here, the denoised image is provided as input and is accomplished by using DFEDC [21], where the loss function is modified using Exponential Baikal Loss. The Exponential Baikal Loss is designed by merging Baikal Loss [22] and Exponential Loss [23]. Additionally, DFEDC is trained by utilizing the proposed ALStarOA, which is developed by merging ALA and SFOA.

Architecture of Dual Fusion with Enhanced Deformable Convolution Network

This is a U-shaped hierarchical model, which contains a dual fusion module for integration, an encoder for feature extraction, and a decoder for reconstruction. DFEDC [21] enhances medical image segmentation by fusing global spatial and channel features, expanding receptive fields with structured deformable convolutions, and integrating 2D-3D features for precise boundary detection and multi-scale representation. DFEDC utilizes the denoised image as its primary input. The encoder in DFEDC leverages a pre-trained MaxViT module to extract rich hierarchical features. At the core of the architecture lies a dual fusion mechanism, composed of Global Spatial Fusion (GSF) and Global Channel Fusion (GCF). These modules collaboratively integrate spatial information and multi-scale channel, reinforcing inter-layer relationships and facilitating seamless connectivity between the decoder and encoder.

In the DFEDC architecture, the encoder serves as the foundational component responsible for removing rich and hierarchical features from input medical image. It utilizes a pre-trained MaxViT module, which combines convolutional operations with multi-axis attention to gather both global contextual and local textures relationships. This enables the encoder to generate multi-scale feature representations that are crucial for accurate segmentation.

The fusion strategy, which jointly leverages global channel and spatial features, substantially enhances the model's representational power and segmentation accuracy. GCF facilitates inter-channel interactions within the feature maps, promoting diversity and complementarity across channels. Meanwhile, GSF captures spatial dependencies and structural coherence throughout the image, enabling the model to maintain consistency across regions and better interpret global context. By enforcing pixel-level consistency for similar semantic regions, GSF improves robustness against local noise and deformation.

In the DFEDC architecture, each encoder layer captures distinct levels of information: deeper layers yield richer semantic features at the cost of spatial detail, while intermediate layers retain a balance of semantic depth and fine-grained detail. Spatial information varies across encoder layers: upper layers retain fine-grained details, while deeper layers capture increasingly abstract spatial representations. In the DFEDC architecture, the decoder is composed of

four Enhanced Deformable Convolution Blocks (EDCBs), each structured sequentially with a Structured Deformable Convolution (SDC) module followed by a Hybrid 2D and 3D feature extraction (H23) module. The SDC module plays a critical role in aggregating features across three distinct scales, enabling the system to gather complementary and diverse information.

Structured Deformable Convolution (SDC) module in DFEDC is built upon a Deformable Convolutional Network (DCN) that is structurally enhanced using Inception and Large Kernel Attention (LKA) mechanisms. This design enables the model to effectively collect multi-scale contextual information and significantly enhance its ability to process complex boundaries. To enhance the flexibility and expressive capacity of convolutional operations, the Multi-Input Offset Fusion (MOF) module has been incorporated into the architecture. MOF strengthens the deformable convolution mechanism by fusing multiple feature inputs, which enhances the network's ability to learn offsets and capture multi-scale spatial patterns with greater precision. Hybrid 3D and 2D feature extraction (H23) module is designed to maximize the utilization of both channel and spatial information, thereby improving model's feature representation capabilities. Structurally, it comprises two parallel paths: 3D path and 2D path. The 2D path is responsible for capturing fine-grained local spatial features and modeling short-range dependencies, which are crucial for precise boundary delineation. In contrast, the 3D path focuses on cross-channel interactions, enabling the extraction of global contextual information that supports semantic consistency across regions. By integrating the outputs from both paths, H23 module effectively fuses multi-scale and multi-level features, resulting in a richer and more expressive representation of the input feature map. The segmented output obtained from DFEDC is characterized as G . The structure of the DFEDC is as shown in Fig. 2.

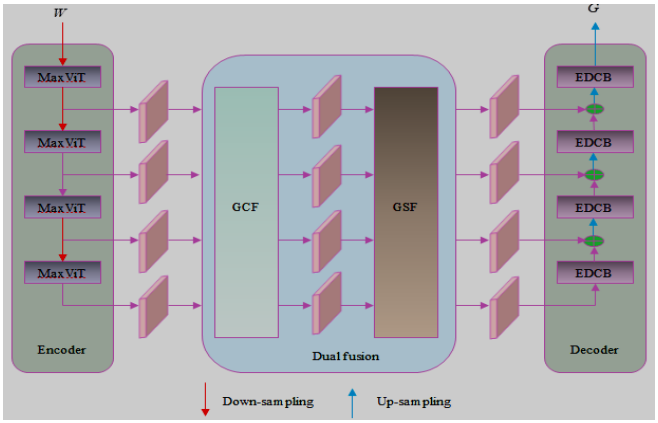

Fig. 2. Structure of DFEDC.

Loss function modification using Exponential Baikal loss

During brain tumor region segmentation, the loss function is modified by using Exponential Baikal Loss, which is derived by fusing Baikal Loss [22] and Exponential Loss [23]. Exponential Baikal loss enhances robustness to noise, sharpens boundary detection, improves convergence, and adapts dynamically to data complexity, making it ideal for precise segmentation and high-dimensional optimization tasks.

Exponential Loss [23] is a margin-sensitive function, which is frequently employed in binary classification tasks such as AdaBoost, where it imposes increasingly severe penalties for confident yet incorrect predictions. The exponential loss B_{EXP} is defined as,

$$B_{EXP} = e^{-PR} \tag{3}$$

where, P stands for predicted boundary pixels and R refers to ground truth boundary pixels. Baikal Loss [22] is a modified loss function designed to enhance segmentation performance, particularly in medical imaging tasks like brain tumor detection. It builds upon traditional loss functions by introducing exponential weighting, which increases sensitivity to misclassified pixels, especially near object boundaries. The Baikal loss B_{Baikal} is mathematically modelled by,

$$B_{Baikal} = \frac{1}{k}\sum_{m=0}^{k}\log\left(R_m\right) - \frac{P_m}{R_m} \tag{4}$$

where, k signifies number of classes and m refers to indexes in every class.

The overall loss function (B) is obtained by combining both exponential loss and Baikal loss and is given by,

$$B = \lambda_1 B_{EXP} + \lambda_2 B_{Baikal} \tag{5}$$

wherein, λ_1 and λ_2 denotes scaling factors.

Training of DFEDC Network using Artificial LemStar Optimization Algorithm

The segmentation performance is further enhanced by applying the ALStarOA to train DFEDC [21]. Here, the ALStarOA is a novel algorithmic approach formulated by incorporating ALA and SFOA. The SFOA is a nature-inspired metaheuristic algorithm devised by considering the distinctive behaviors of starfish, such as regeneration, predation, and exploratory movement. SFOA demonstrates rapid convergence during exploitation and maintains computational efficiency during exploration. The ALA is a novel bio-inspired metaheuristic designed to address complex engineering optimization problems. Modeled after the behavioral patterns of lemmings, Lemmings are diminutive rodents indigenous to Arctic tundra ecosystems, distinguished by short tails, specialized flattened claw, and small ears on the first digit of their forefeet, which aids in snow excavation. As herbivores, their diet is primarily composed of mosses and grasses, supplemented by leaves, lichens, bulbs, subterranean roots, and berries. Lemmings exhibit proficient burrowing behavior, constructing insulated tunnels for shelter and food storage. Their ecological habits encompass foraging, excavation, seasonal migration, and predator avoidance, reflecting their adaptive strategies in natural predators. Combining ALA with SFOA boosts convergence, balances exploration-exploitation, adapts parameters dynamically, and avoids local minima, ideal for complex tasks in brain tumor segmentation and image analysis. The stages followed by ALStarOA are described below.

Initialization: ALStarOA is a population-driven optimizer that starts by initializing the spatial coordinates of all agents. Firstly, a group of lemmings is initiated, each symbolizing a distinct solution to the optimization problem. The population $\overrightarrow{D}$ is stated by,

$$\overrightarrow{D} = \begin{bmatrix} d_{1,1} & d_{1,2} & \cdots & d_{1,D\mathrm{im}-1} & d_{1,D\mathrm{im}} \\ d_{2,1} & d_{2,2} & \cdots & d_{2,D\mathrm{im}-1} & d_{2,D\mathrm{im}} \\ \cdots & \cdots & d_{b,p} & \cdots & \cdots \\ \vdots & \vdots & \vdots & \vdots & \vdots \\ d_{H-1,1} & d_{H-1,2} & \cdots & d_{H-1,D\mathrm{im}-1} & d_{H-1,D\mathrm{im}} \\ d_{H,1} & d_{H,2} & \cdots & d_{H,D\mathrm{im}-1} & d_{H,D\mathrm{im}} \end{bmatrix} \tag{6}$$

Foe every dimension, decision variable $d_{b,p}$ is articulated as,

$$d_{b,p} = lb_p + rand \times \left(ub_p - lb_p\right), b = 1,2,\ldots,H, p = 1,2,\ldots,D\mathrm{im} \tag{7}$$

wherein, $rand$ denotes a random number ranges within $[0,1]$, population size is characterized as H , lb_p and ub_p specifies the lower limit and upper limit of p^{th} dimension, and overall dimensions is indicated as $D\mathrm{im}$.

The loss function is used to evaluate fitness function and is explained in section 3.3.2.

Exploration (Long-distance migration): Lemmings naturally travel long distances when food runs low, because there are too many of them in one place. They find new areas by using their sense of direction and by following random members of their group, hoping to discover places with more food and better living conditions. The long-distance migration behavior is articulated as,

$$\overrightarrow{D_b}(n+1) = \overrightarrow{D_{best}}(n) + I \times \overrightarrow{BM} \times \left[\overrightarrow{M} \times \left(\overrightarrow{D_{best}}(n) - \overrightarrow{D_b}(n)\right) + \left(1-\vec{S}\right) \times \left(\overrightarrow{D_b}(n) - \overrightarrow{D_h}(n)\right)\right] \tag{9}$$

Here, current ideal solution is denoted as $\overrightarrow{D}_{best}(n)$, an integer index among H and 1 is given by h, I symbolizes a flag to change search direction, Brownian motion is specified as $\overrightarrow{BM}$, an arbitrarily selected search individual from the population is indicated as $\overrightarrow{D_h}(n)$, the present position of the b^{th} search agent is denoted as $\overrightarrow{D_b}(n)$, position of b^{th} search agent at $(n+1)^{th}$ iteration is designated as $\overrightarrow{D_b}(n+1)$, and $\vec{S}$ designates a vector of size $1\times D$im.

Digging holes: In this phase, lemmings engage to build elaborate burrow systems to store food and seek refuge. Each new tunnel is carved out at random, guided by current burrow's location and proximity of nearby individuals in population. The behavior of digging holes is articulated by,

$$\overrightarrow{D_b}(n+1)=\overrightarrow{D_b}(n)+I\times K\times\left[\overrightarrow{D}_{best}(n)-\overrightarrow{D_f}(n)\right] \tag{10}$$

wherein, a random integer index value within 1 and H is denoted as f, a random number concerning present iteration number is represented as K, and a search individual chosen arbitrarily from population is signified as $\overrightarrow{D_f}$. SFOA [25] is a bio-inspired metaheuristic designed to solve complex optimization problems by mimicking the unique behaviors of starfish, particularly their exploration, preying, and regeneration strategies. Moreover, SFOA offers adaptive search, strong global exploration, fast convergence, resilience, and high accuracy across diverse, high-dimensional optimization problems. SFOA incorporated with ALA improves optimization by adaptively tuning parameters, accelerating convergence, enhancing exploration, and avoiding local minima traps. From SFOA,

$$\overrightarrow{E_b}(n+1)=\overrightarrow{D_b}(n)+e_1\left[\overrightarrow{D}_{best}(n)-\overrightarrow{D_b}(n)\right]\cos\theta,\ \ i\le 0.5 \tag{11}$$

$$\overrightarrow{D_b}(n+1)=\overrightarrow{E_b}(n+1)\ \ lb_p\le\overrightarrow{E_b}(n+1)\le ub_p \tag{12}$$

where, $\overrightarrow{E_b}(n+1)$ the updated location of starfish, e_1 refers to the scaling coefficient, $\overrightarrow{D}_{best}(n)$represents best starfish's location, $\overrightarrow{D_b}(n)$ refers to present starfish's position, $\theta=\frac{\pi}{2}\frac{n}{T_{max}}$ and $i\in(0,1)$.

Substituting equation (11) in equation (12),

$$\overrightarrow{D_b}(n+1)=\overrightarrow{D_b}(n)\left[1-e_1\cos\theta\right]+e_1*\overrightarrow{D}_{best}\cos\theta \tag{13}$$

$$\overrightarrow{D_b}(n)=\frac{\overrightarrow{D_b}(n+1)-e_1*\overrightarrow{D}_{best}\cos\theta}{1-e_1\cos\theta} \tag{14}$$

Substituting expression (14) in expression (10),

$$\overrightarrow{D_b}(n+1)=\left[\frac{\overrightarrow{D_b}(n+1)-e_1*\overrightarrow{D}_{best}\cos\theta}{1-e_1\cos\theta}\right]+I\times K\times\left[\overrightarrow{D}_{best}(n)-\overrightarrow{D_f}(n)\right] \tag{15}$$

$$\frac{\overrightarrow{D_b}(n+1)\left[1-e_1\cos\theta-1\right]}{1-e_1\cos\theta}=\frac{\left(I\times K\times\left[\overrightarrow{D}_{best}(n)-\overrightarrow{D_f}(n)\right]\right)(1-e_1\cos\theta)-e_1*\overrightarrow{D}_{best}\cos\theta}{1-e_1\cos\theta} \tag{16}$$

The updated equation for ALStarOA is given by,

$$\overrightarrow{D_b}(n+1)=\frac{1}{e_1\cos\theta}\left[e_1*\overrightarrow{D}_{best}\cos\theta-\left(I\times K\times\left[\overrightarrow{D}_{best}(n)-\overrightarrow{D_f}(n)\right]\right)(1-e_1\cos\theta)\right] \tag{17}$$

Foraging for food: During this behavioral phase, lemmings show erratic movement patterns within their burrow systems, relying on their acute olfactory and auditory senses to locate food. Their foraging remains spatially limited, governed by the proximity of available resources. To optimize intake, they employ stochastic exploratory strategies within this confined zone. The spiral wrapping strategy considered for foraging of food is computed as,

$$\overrightarrow{D_b}(n+1)=D_{best}(n)+I\times spiral\times rand\times\overrightarrow{D_b}(n) \tag{18}$$

wherein, spiral shape of random search during foraging is represented as $spiral$.

Evading natural predators: Lemmings respond to danger with swift, calculated movements. Their burrows act as safe havens, and when predators approach, they dash back with impressive speed. To further ensure escape, they use clever misdirection to throw off their pursuers. The behaviour of evading a natural predator is mathematically formulated as,

$$\overrightarrow{D_b}(n+1)=\vec{D}_{best}(n)+I\times J\times Levy(D\text{im})\times\left[\vec{D}_{best}(n)-\vec{D}_b(n)\right] \tag{19}$$

Here, the Levy flight function is designated as $Levy(D\text{im})$ and the escape coefficient of lemmings is specified as J .

Table I.

Algorithm for ALStarOA

Pseudocode of ALStarOA
Input: Maximum iteration T_{max} , dimension size D im , and Population size H ,
Output: Fitness value N_{best} and global ideal solution $\vec{D}_{best}$
Initialize every lemming position arbitrarily, $\vec{d}_b$ $(b=1,2,\ldots,H)$
Evaluate the fitness function of the entire population
Estimate the present optimal solution $\vec{D}_{best}$
$n=1$
while $n\le T_{max}$ **do**
for each search individual $\vec{D}_b$ **do**
if energy factor $E>1$ **then**
Exploration phase
if $rand<0.3$ **then**
Modify lemming's location using expression (9)
else
Modify lemming's current location exploiting expression (17)
end
else
Exploitation phase
if $rand<0.5$ **then**
Update present lemming individual's location utilizing expression (18)
else
Upgrade current lemming individual's position using expression (19)
end
end
end
Re-estimate fitness of entire lemming individuals
Update the ideal optimal gained so far $\vec{D}_{best}$
$n=n+1$
end

Re-evaluation of fitness: The loss function specified in section 3.3.2 serves as the fitness evaluation function, guiding the search for the optimal solution. When a more favourable candidate emerges, the current solution is accordingly updated.

Termination: The algorithm proceeds through iterative steps, continuously refining solutions until an optimal candidate surpassing previous iterations is identified. Table 1 presents the algorithm for ALStarOA.

The integration of SFOA with ALA significantly improves optimization performance by expediting convergence, enhancing local search capabilities, and enabling dynamic parameter adaptation. This synergy also strengthens segmentation outcomes by avoiding local optima and promoting faster convergence.

4. Results And Discussion

The DFEDC_ALStarOA model for brain tumor segmentation is implemented in MATLAB using the BraTS dataset [26]. MRI scans sourced from multiple institutions, encompassing both High-Grade Gliomas (HGG) and Low-Grade Gliomas (LGG). In total, the training set includes 335 cases, comprising of 259 HGG and 76 LGG, while the validation set consists of 125 cases. The MRI data of each subject includes four imaging modalities: T2-weighted, Fluid Attenuated Inversion Recovery (FLAIR), native T1-weighted and post-contrast T1-weighted (T1Gd).

The efficacy of DFEDC_ALStarOA in segmenting brain tumors is measured using performance metrics, like IOU, Dice coefficient, and Segmentation accuracy.

Segmentation accuracy*:* It defines how precisely the DFEDC_ALStarOA can categorize each pixel in an image into its accurate category during image segmentation tasks. The segmentation accuracy is defined as,

$$Segmentation\ \ Accurracy=\frac{R_1+Q_1}{S_1+Q_1+F_1+R_1} \tag{20}$$

where, S_1 represents false positive rate, R_1 denotes true positive rate, Q_1 embodies true negative rate, and R_1 indicates false negative rate.

***Dice coefficient*:** The Dice coefficient quantifies overlap among ground truth and predicted tumor regions.

The dice coefficient is computed as,

$$Dice\,coefficient = \frac{2|T_1 \cap Z_1|}{|T_1| + |Z_1|} \tag{21}$$

wherein, T_1 indicates a cluster of predicted tumor pixels, $|T_1 \cap Z_1|$ denotes pixel count common in both predicted and ground truth tumor areas. $|T_1|$ stipulates the number of pixels in predicted tumor region and $|Z_1|$ represents pixel counts in ground truth tumor area.

***IOU*:** It is employed to assess segmentation accuracy of by computing the ratio of the intersection to union of ground truth and predicted masks. It is computed by,

$$IOU = \frac{|T_1 \cap Z_1|}{|T_1 \cup Z_1|} \tag{22}$$

The simulation parameters for DFEDC and ALStarOA's techniques are tabulated in Table 2 and Table 3 respectively.

Table II. Parameters of DFEDC Model

Parameters	**Values**
Number of channels	64
Activation	SoftMax
Kernel size	3 X 3
Loss function	Exponential Baikal loss
Optimizer	ALStarOA
Strides	2
Batch size	32

The image outcomes obtained by DFEDC_ALStarOA for segmenting brain tumors when applied to image size of 256 x 256. Fig. 3(a), shows the input image, Fig. 3(b) exemplifies denoised image, the segmented image is shown in Fig 3(c), and in Fig 3(d), classified image is presented.

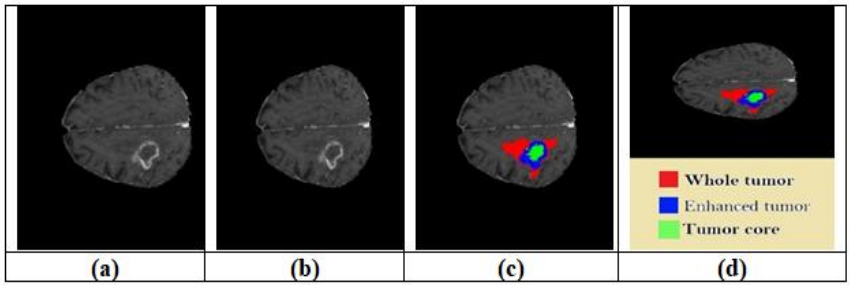

Fig. 3. Segmentation for the image size of 256 x 256; (a) input image, (b) denoised image, (c) segmented image, and (d) classified output image.

Fig. 4 depicts the results for the image of size 64 x 64. Fig 4(a) presents input image, Fig 4(b) is the denoised image, Fig. 4(c) is the segmented image and Fig 4(d) shows the classified output image.

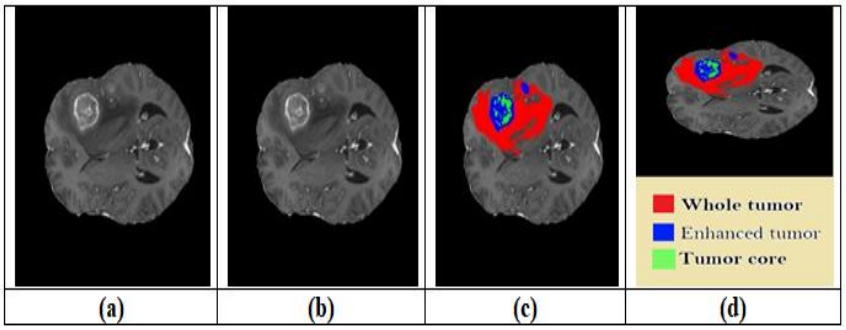

Fig. 4. Image outputs for the image size of 64 x 64; (a) input image, (b) denoised image, (c) segmented image, and (d) classified output image.

Table III.

Parameters of ALStarOA model

Parameters	Details	Values
$T_{\max}$	Maximum Iteration	500
$d_{b,p}$	Decision variable	30
H	Population size	50
$rand$	Random	Random numbers between (0,1)
K		random numbers between (-1,1)
h	Integer index	Between (1,50)
f		Random numbers between (0,1)
v		Random numbers between (0,1)
β	constant	1.5

Comparative Analysis

The effectiveness of DFEDC_ALStarOA for segmenting brain tumors is analyzed by comparing its performance with prevailing approaches, namely UNet [16], MultiModNet [3], LGM+DAP+RDKIM [17] and YOLO-BT [8].

Comparative analysis for the image size of 64 x 64*:* In Fig 5(a) segmentation accuracy is depicted. With 1000 number of images, DFEDC_ALStarOA achieved a segmentation accuracy of 91.880%, and the segmentation accuracy recorded by existing techniques, named U-Net is 81.980%, MultiModNet is 83.910%, LGM+DAP+RDKIM is 86.990%, and YOLO-BT is 88.989%. Now, DFEDC_ALStarOA is improved by 3.15% than U-Net considering segmentation accuracy. Fig. 5(b) presents the dice coefficient. The dice coefficient recorded by DFEDC_ALStarOA

is 91.888% and existing models, including U-Net is 81.988%, MultiModNet is 83.998%, LGM+DAP+RDKIM is 85.999%, and YOLO-BT is 87.999%, with 2000 images. Compared to MultiModNet, the developed DFEDC_ALStarOA demonstrated a 4.23% improvement in Dice performance. In Fig. 5(c) IOU is portrayed. The IOU obtained by the designed DFEDC_ALStarOA is 94.877%, and prevailing techniques, such as U-Net is 85.888%, MultiModNet is 88.888%, LGM+DAP+RDKIM is 89.910%, and YOLO-BT is 92.888% when the number of images is 3000. The proposed DFEDC_ALStarOA recorded a 4.42% higher IOU than LGM+DAP+RDKIM.

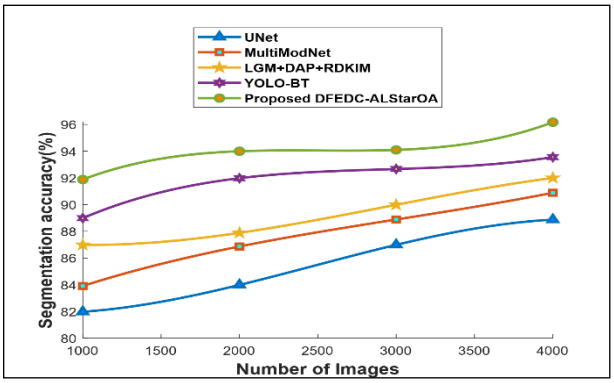

(a)

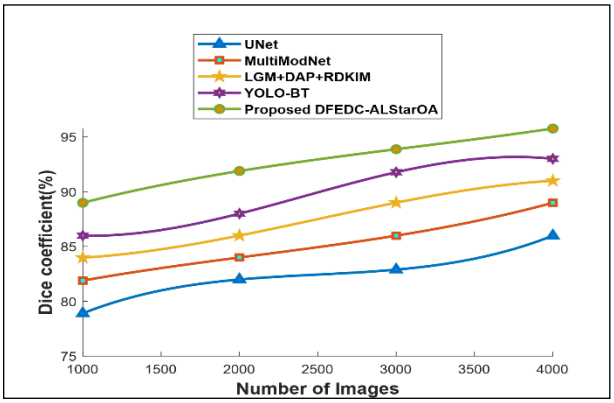

(b)

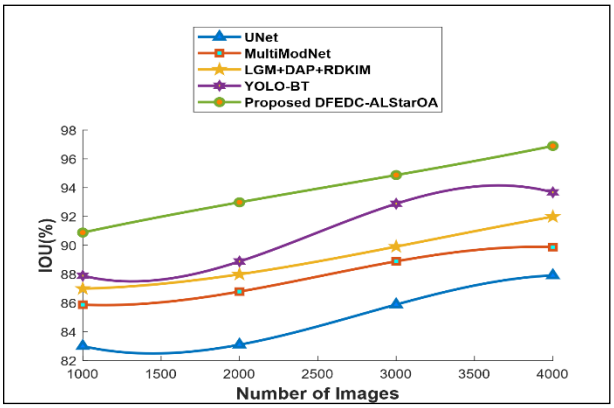

Fig. 5 Estimation of DFEDC_ALStarOA for segmenting brain tumors based on image size of 64 x 64; (a) segmentation accuracy, (b) dice coefficient, and (c) IOU.

Comparative analysis for the image size of 128 x 128: In Fig. 6(a), the assessment of DFEDC_ALStarOA about segmentation accuracy is portrayed. With a number of images as 4000, the proposed method achieved a segmentation accuracy of 96.590%, and prevailing methods, like U-Net is 90.988%, MultiModNet is 91.888%, LGM+DAP+RDKIM is 92.989%, and YOLO-BT is 94.666%. Now, the proposed method out performed MultiModNet by a margin of 3.19% in segmentation accuracy. In Fig. 6(b), the proposed method recorded a Dice coefficient of 91.879%, when the number of images is 1000, and the value achieved by the existing techniques, including U-Net is 81.888%, MultiModNet is 83.989%, LGM+DAP+RDKIM is 85.990%, and YOLO-BT is 88.887%. When compared specifically to U-Net, the proposed method shows an improvement of 3.26%. In Fig. 6(c), analysis of DFEDC_ALStarOA in terms of IOU results is presented, with 2000 images, the proposed model attained an IOU of 94.899%, and the IOU attained by the existing techniques, namely U-Net 86.878%, MultiModNet 87.999%, LGM+DAP+RDKIM 90.988%, and YOLO-BT 92.677%. Compared to LGM+DAP+RDKIM, DFEDC_ALStarOA demonstrated a notable 3.3% improvement in IOU.

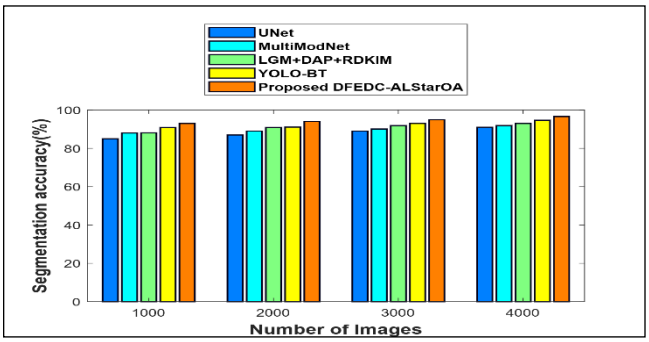

(a)

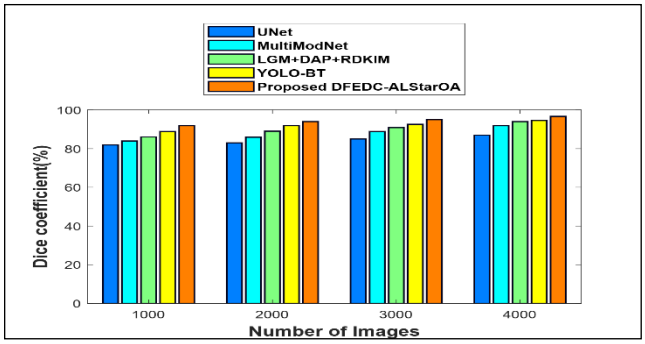

(b)

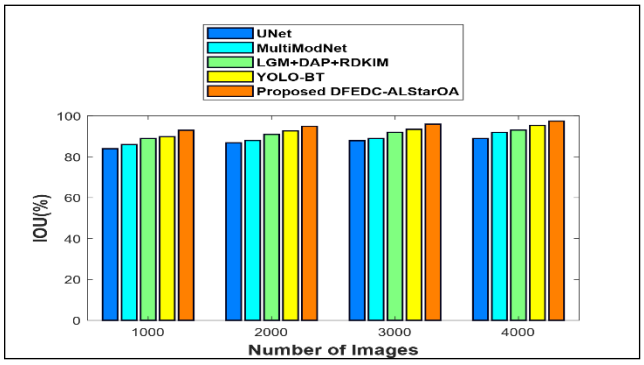

Fig. 6. Assessment for the image size of 128 x 128; (a) segmentation accuracy, (b) dice coefficient, and (c) IOU

Comparative valuation for the image size of 256 x 256: In Fig 7(a), the estimation of DFEDC_ALStarOA for segmentation accuracy is exhibited. By considering number of images as 3000, segmentation accuracy obtained by designed DFEDC_ALStarOA is 95.988%, and prevailing approaches, namely U-Net is 89.988%, MultiModNet is 90.988%, LGM+DAP+RDKIM is 91.099%, and YOLO-BT is 93.988%. Here, the segmentation accuracy of DFEDC_ALStarOA is improved by 2.13% over U-Net. Fig 7(b) highlights the assessment of DFEDC_ALStarOA concerning dice coefficient. The dice coefficient gained by established DFEDC_ALStarOA is 97.158% and existing approaches, like U-Net is 91.877%, MultiModNet is 92.989%, LGM+DAP+RDKIM is 93.887%, and YOLO-BT is 95.555% by using 4000 images. In this case, the dice coefficient of DFEDC_ALStarOA is enhanced higher by 3.06% than LGM+DAP+RDKIM. Lastly, Fig 7(c) presents the analysis for 1000 images. For this image size, the IOU obtained by the proposed method is 93.999% and prevailing frameworks, like U-Net is 85.899%, MultiModNet is 87.988%, LGM+DAP+RDKIM is 89.990%, and YOLO-BT is 90.998%. This demonstrates that the IOU of DFEDC_ALStarOA is improved higher by 3.19% relative to MultiModNet.

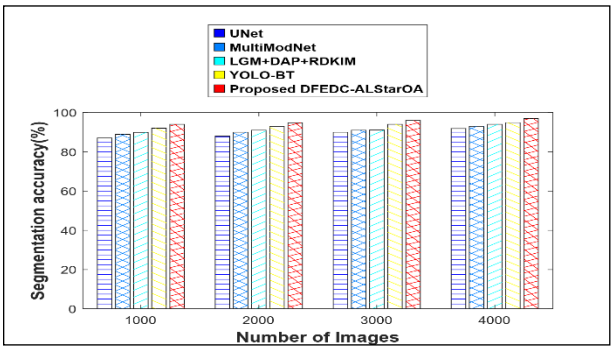

(a)

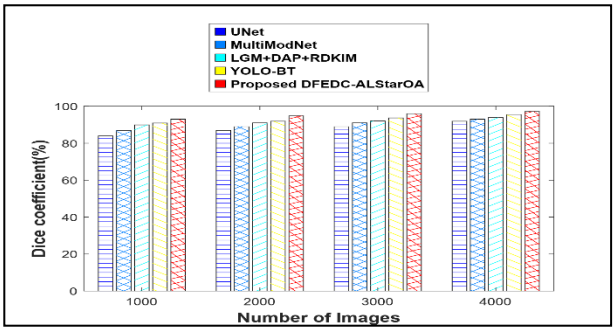

(b)

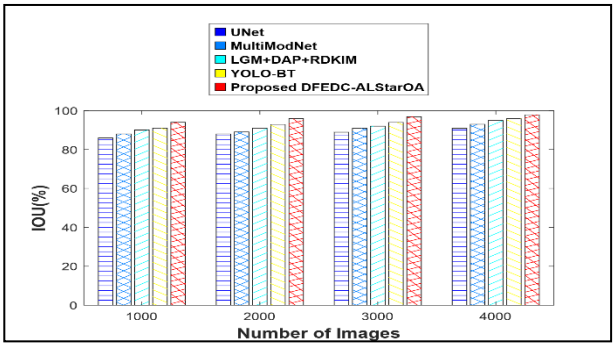

(c)

Fig. 7. Valuation for the image size of 256 x 256; (a) segmentation accuracy, (b) dice coefficient, and (c) IOU.

Comparative valuation for the image size of 512 x 512: The comparative analysis for the image size of 512 x 512 is shown in Fig. 8. In Fig 8(a), shows the analysis for the image size of 2000, the segmentation accuracy of the proposed method is 95.988%, whereas prevailing models, like MultiModNet is 90.988%, U-Net is 89.988%, LGM+DAP+RDKIM is 92.899%, and YOLO-BT is 93.990%. Notably, DFEDC_ALStarOA shows an improvement of 2.51% over LGM+DAP+RDKIM. Fig 8(b) exhibits the analysis of DFEDC_ALStarOA in regard to the dice coefficient. When the number of images is 3000, the dice coefficient attained by DFEDC_ALStarOA is 96.777%, and prevailing methods, namely U-Net is 90.988%, MultiModNet is 91.988%, LGM+DAP+RDKIM is 92.989%, and YOLO-BT is 94.544%. This reflects that DFEDC_ALStarOA attained a 2.48% better dice coefficient than YOLO-BT.

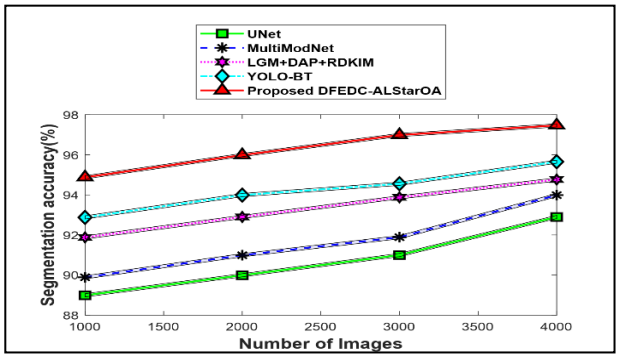

(a)

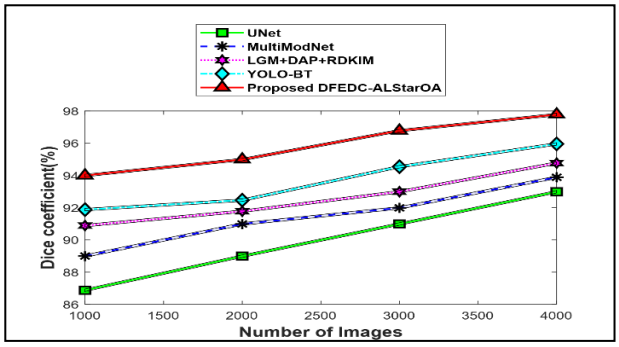

(b)

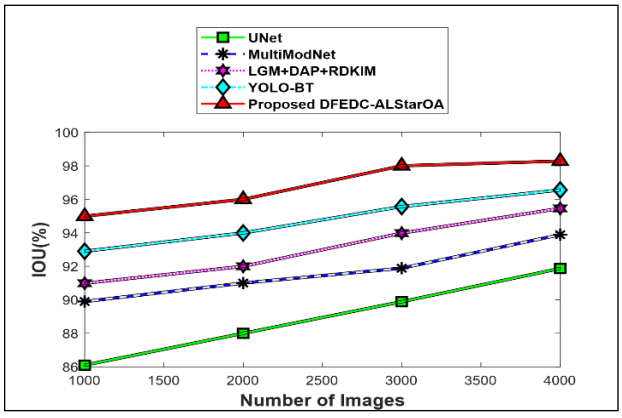

(c)

Fig. 8. Estimation for the image size of 512 x 512; (a) segmentation accuracy, (b) dice coefficient, and (c) IOU.

Fig. 8(c) shows the results for the 4000 images, the IOU attained by the developed method is 98.280%, and prevailing models, including U-Net is 91.870%, MultiModNet is 93.888%, LGM+DAP+RDKIM is 95.454%, and YOLO-BT is 96.555%. This represents that DFEDC_ALStarOA achieves an IOU higher by 2.66% over MultiModNet.

The comparison of DFEDC_ALStarOA with various metrics by varying image sizes is shown in Table 4. For the 4000, the segmentation accuracy acquired by DFEDC_ALStarOA is 97.468%, and existing methods like MultiModNet is 93.988%, LGM+DAP+RDKIM is 94.766%, U-Net is 92.898%, and YOLO-BT is 95.655%. Likewise, the dice coefficient obtained by prevailing methods, like U-Net is 92.987%, MultiModNet is 93.887%, LGM+DAP+RDKIM is 94.766%, and YOLO-BT is 95.956%, and the proposed DFEDC_ALStarOA achieves dice coefficient of 97.778%. Also, the IOU acquired by designed DFEDC_ALStarOA is 98.280%, and prevailing frameworks, namely U-Net is 91.870%, MultiModNet is 93.888%, LGM+DAP+RDKIM is 95.454%, and YOLO-BT is 96.555%. DFEDC improves tumor boundary detection, captures multi-scale features, adapts to irregular shapes, and boosts segmentation robustness.

Table IV. Performance comparison of the proposed model with the existing models.

Image Size	*Metrics*	*UNet*	*MultiModNet*	*LGM+DAP +RDKIM*	*YOLO-BT*	*Proposed DFEDC_ ALStarOA*
64x64	*Segmentation accuracy (%)*	*88.877*	*90.888*	*91.999*	*93.555*	*96.169*
	Dice coefficient (%)	*85.988*	*88.990*	*90.999*	*92.999*	*95.766*
	IOU (%)	*87.910*	*89.879*	*91.988*	*93.678*	*96.899*
128x128	*Segmentation accuracy (%)*	*90.988*	*91.888*	*92.989*	*94.666*	*96.590*
	Dice coefficient (%)	*86.980*	*91.879*	*93.980*	*94.555*	*96.679*
	IOU (%)	*88.988*	*91.980*	*93.100*	*95.347*	*97.469*
256x256	*Segmentation accuracy (%)*	*91.877*	*92.987*	*93.9898*	*94.877*	*96.909*
	Dice coefficient (%)	*90.8977*	*92.988*	*94.8878*	*95.876*	*97.878*
	IOU (%)	*83.483*	*85.005*	*87.275*	*89.355*	*90.585*
512x512	*Segmentation accuracy (%)*	*92.898*	*93.988*	*94.766*	*95.655*	***97.467***
	Dice coefficient (%)	*92.987*	*93.887*	*94.766*	*95.955*	***97.777***
	IOU (%)	*91.872*	*93.8878*	*95.4544*	*96.555*	***98.279***

5. Conclusion

Segmenting the tumor allows clinicians to accurately determine its size, shape, location, and boundaries. This information is critical for distinguishing between tumor types and understanding tumor heterogeneity. Additionally, the proposed DFEDC model is trained utilizing a newly developed optimization algorithm, ALStarOA, which combines the strengths of ALA and SFOA. The proposed DFEDC_ALStarOA obtains higher dice coefficient of 97.777%, IOU of 98.2799%, and segmentation accuracy of 97.4678%. In the future, this approach aims to leverage transfer learning, thereby improving its generalization.

Declarations

Ethical Approval

This study was conducted by ethics, and All procedures adhered to ethical guidelines for research are followed.

Consent for Publication Participants.

Consent for publication was given by all participants

Competing Interests

The authors have no competing interests to declare.

References:

1. Md. Eshmam Rayed S.M. Sajibul Islam, Sadia Islam Niha, Jamin Rahman Jim, Md Mohsin Kabir, M.F. Mridha " Deep learning for medical image segmentation: State-of-the-art advancements and challenges", Journal of Imaging, Informatics in Medicine Unlocked, vol. 47, pp. 101504, 2024.
2. E. Zarenia, A. A. Far and K. Rezaee, "Automated multi-class MRI brain tumor classification and segmentation using deformable attention and saliency mapping," Scientific Reports, vol. 15, no. 1, p. 8114, 2025.
3. T. J and T. T, "MultiModNet: An automated multimodal network for brain tumor volume determination and grading with three-dimensional u-net and deformable voxel fusion," Biomedical Signal Processing and Control, vol. 103, p. 107469, 2025.
4. A. Gooya, K. M. Pohl, M. Bilello, G. Biros and C. Davatzikos, "Joint segmentation and deformable registration of brain scans guided by a tumor growth model,"in Medical Image Computing and Computer-Assisted Intervention–MICCAI, Toronto, Canada, 2011.
5. K. Hemalatha, Alfred Dharmaraj A, P.R. Vishnu Vardhan, Hari Hara Sudhan S, " Mutual Information Clustering and Segmentation framework with Masking Noise Few-Shot Domain Adaptation ResNet for multi-modal brain tumor classification," Biomedical Signal Processing and Control, vol. 114, pp. 109290, 2026.
6. Sumit Raghuvamshi, Ambuj Sukhad, Akhtar Rasool, Vikas,Kumar Meena, Abhishek Jadhav, Katravath Shivakarthi. “Early Detection of Brain Tumor from MRI Images Using Different Machine Learning Techniques," Procedia Computer Science, vol. 235, pp. 3094-3104, 2024.
7. M. Havaei, A. Davy, D. Warde-Farley, A. Biard, A. Courville, Y. Bengio, C. Pal, P M Jodoin and H. Larochelle, "Brain tumor segmentation with deep neural networks," Medical Image Analysis, vol. 35, pp. 18-31, 2017.
8. Almetwally M. Mostafa Almetwally M. Mostafa Zakariah and Eman Abdullah Aldakheel, "Brain Tumor Segmentation Using Deep Learning on MRI Images," Diagnostics, vol. 13, no. 9, pp. 1562, 2023.
9. Z. Liu, L. Tong, L. Chen, Z. Jiang, F. Zhou, Q. Zhang, X. Zhang, Y. Jin and H. Zhou, "Deep learning based brain tumor segmentation: a survey," Complex and intelligent systems, vol. 9, no. 1, pp. 1001-1026, 2023.
10. Pooja Kataria, Ayush Dogra, Mili Gupta, Tripti Sharma and Bhawna Goyal, “Trends in DNN Model based Classification and Segmentation of Brain Tumor Detection," The Open Neuroimaging Journal, vol. 16, 2024.
11. G. S. "Brain Tumor classification using the Probabilistic-Deformable Fuzzy system and RideNN," Multimedia Research, vol. 5, no. 4, 2024.
12. Zain Ul Abidin1, Rizwan Ali Naqvi, Amir Haider, Recent deep learning-based brain tumor segmentation models using multi-modality MRI: a prospective survey,” Frontiers in Bioengineering and Biotechnology, DOI: 10.3389/fbioe.2024.1392807, 2024.
13. P. K. Tiwary, P. Johrl, A. KATIYAR and M. K. CHHIPA, "Deep Learning-Based MRI Brain Tumor Segmentation with EfficientNet-Enhanced UNet," IEEE Access, 2025.
14. [14] A. M. Mostafa, M. Zakariah and E. Aldakheel, "Brain tumor segmentation using deep learning on MRI images," Diagnostics, vol. 13, no. 9, p. 1562, 2023.
15. M. F. ALMUFAREH, M. IMRAN, A. KHAN, M. HUMAYUN and M. ASIM, "Automated brain tumor segmentation and classification in MRI using YOLO-based deep learning," IEEE Access, vol. 12, pp. 16189-16207, 2024.
16. . M. Obayya, A. Alshuhail, K. Mahmood, M. H. Alanazi, M. Alqahtani, N. O. Aljehane, H. Almansour and M. A. Al-Hagery, "A novel U-net model for brain tumor segmentation from MRI images," Alexandria Engineering Journal, vol. 126, pp. 220-230, 2025.
17. Z. Li, Y. Zhang, . H. Li, Y. Chai and Y. Yang, "Deformation-aware and reconstruction-driven multimodal representation learning for brain tumor segmentation with missing modalities," Biomedical Signal Processing and Control, vol. 91, p. 106012, 2024.
18. X. Ma, M. Tian, J. Ye, Y. Liao, Y. Chen, C. Xie, R. Li, P. Li, J. Wang, X. Xu and X. Lai, "Dual examiner consistency learning with dynamic receptive fields and class-balance refinement for Barely-supervised brain tumor segmentation," Displays, vol. 88, p. 103054, 2025.
19. M. Xiong, A. Wu, Y. Yang and Q. Fu, "Efficient Brain Tumor Segmentation for MRI Images Using YOLO-BT," Sensors, vol. 25, no. 12, p. 3645, 2025.

20. Afnan M. Alhassan, Nouf I. Altmami, “An efficient Alzheimer’s disease detection using optimized hybrid light GBM-based CNN," Ain Shams Engineering Journal, vol. 16, no. 12, pp. 103811, 2025.

21. X. Fang, Y. Pan and Q. Chen, "DFEDC: Dual fusion with enhanced deformable convolution for medical image segmentation," Image and Vision Computing, vol. 151, p. 105277, 2024.

22. Ying H, Song M, Tang Y, “Enhancing deep neural network training efficiency and performance through linear prediction,” Scientific Reports, vol. 14, pp. 15197, DOI: 10.1038/s41598-024-65691-0 2024.

23. Fatemeh Chahkoutahi, Mehdi Khashei, Naser Molaverdi, “Loss functions in classification: An comprehensive overview and comparative study," Applied Soft Computing, vol. 184, pp. 113778, 2025.

24. Y. Xiao, . H. Cui, . R. A. Khurma and . P. A. Castillo, "Artificial lemming algorithm: a novel bionic meta-heuristic technique for solving real-world engineering optimization problems," Artificial Intelligence Review, vol. 58, no. 3, p. 84, 2025.

25. C. Zhong, G. Li, Z. Meng, H. Li, A. R. Yildiz and S. Mirjalili, "Starfish optimization algorithm (SFOA): a bio-inspired metaheuristic algorithm for global optimization compared with 100 optimizers," Neural Computing and Applications, vol. 37, no. 5, pp. 3641-3683, 2025.

26. The Brain_Tumor_Segmentation_BraTS_2024, Available: https://www.kaggle.com/datasets/aryashah2k/brain-tumor-segmentation-brats-2024..